GEOPERSIA

Accepted Manuscript

Leveraging EDA, Fractal Analysis, SFA, and GMPI for Identifying Geochemical Anomalies in Siah Cheshmeh Ophiolite Area, NW Iran

Alireza Haghighi, Ali Imamalipour, Samaneh Barak

DOI: 10.22059/GEOPE.2024.380369.648769

Receive Date: 12 August 2024
Revise Date: 31 October 2024
Accept Date: 09 November 2024

Leveraging EDA, Fractal Analysis, SFA, and GMPI for Identifying Geochemical Anomalies in Siah Cheshmeh Ophiolite Area, NW Iran

Alireza Haghighi, Ali Imamalipour *, Samaneh Barak

Department of mining engineering, Urmia university, Urmia, Iran

Received: 12 August 2024, Revised: 31 October 2024, Accepted: 09 November 2024

Abstract
This study focuses on the integration of geochemical data analysis methods to enhance mineral exploration in the Siah Cheshmeh region of the Khoy Ophiolite in northwestern Iran. Initially, all preprocessing steps were applied to the geochemical data to ensure its quality and accuracy before proceeding with the main analysis. Staged Factor Analysis (SFA) was then employed to identify key elements closely related to mineralization processes, such as Au, Cu, Fe, Mn, Zn, Cr, and Ni, due to their significant roles in mineral enrichment and deposit formation. These elements were subsequently analyzed using Exploratory Data Analysis (EDA) and fractal modeling techniques to differentiate background from anomaly concentrations, effectively detecting high-anomaly areas indicative of mineral-rich zones. For example, the anomaly area for manganese using the fractal method was determined to be 4,551,879 square meters, compared to 22,107,400 square meters obtained using EDA, highlighting the fractal method's higher precision in mapping anomalies. The SFA approach was further refined using the Geochemical Mineralization Potential Index (GMPI), with calculations performed for the associations $GMPI_{Au\text{-}Cu\text{-}Fe\text{-}Mn\text{-}Zn}$ and $GMPI_{Cr\text{-}Ni}$. GMPI values were determined based on the 95% cumulative frequency, with additional thresholds at 99% and 97.5% to highlight higher-intensity anomalies. This comprehensive integration of SFA, EDA, fractal modeling, and GMPI methods produced detailed geochemical maps that precisely identify prospective exploration areas, emphasizing regions with high mineral potential. The study demonstrates the effectiveness of combining these techniques to guide focused geochemical investigations for mineral exploration.

Keywords: Geochemical Exploration, SFA, Fractal Modeling, EDA, GMPI, Siah Cheshmeh, Iran.

Introduction

Exploratory Data Analysis (EDA) is vital in geochemistry for distinguishing anomalies from background levels in geological datasets. EDA involves using statistical and graphical techniques to summarize data, identify patterns, detect outliers, and formulate hypotheses, laying the groundwork for more advanced analyses (Yusta et al., 1998; Shuguang et al., 2015; Sanchez Siachoque, 2023). Key EDA techniques in geochemistry include: (1) Descriptive Statistics: Measures like mean, median, and standard deviation provide a basic understanding of data distribution, (2) Graphical Tools: Histograms, boxplots, scatter plots, and Q-Q plots help visualize data distribution and identify trends, (3) Spatial Analysis: Techniques like geochemical mapping and contour plots are used to visualize the geographical distribution of geochemical data, (4) Multivariate Methods: Principal Component Analysis (PCA) and cluster analysis are employed to explore the relationships between multiple variables simultaneously.

* Corresponding author e-mail: A.imamalipour@urmia.ac.ir

These methods collectively enhance the understanding of geochemical distributions and help identify regions with anomalous element concentrations (Imamalipour & Barak, 2019; Ebrahimi & Barak, 2019). By systematically cleaning and preparing data, detecting patterns, visualizing spatial distributions, and applying multivariate analyses, EDA provides a comprehensive approach to separating geochemical anomalies from the background. This process is crucial for guiding detailed analysis, improving the efficiency of mineral exploration, and informing environmental monitoring efforts (Gutierrez et al., 2012; Agharezaei & Hezarkhani, 2016).

Fractals, intricate patterns that are self-similar across different scales, have significant applications in geochemistry. First proposed by Mandelbrot (1982, 1989), fractals provide a powerful framework for analyzing complex and irregular natural phenomena, which traditional Euclidean geometry struggles to address. In geochemistry, fractals help in understanding the spatial and temporal distributions of chemical elements and minerals in the Earth's crust. The fractal nature of geological formations, mineral deposits, and geochemical anomalies reveals underlying patterns that are critical for resource exploration, environmental monitoring, and understanding geological processes (Cheng et al., 1994; Xie & Bao, 2004; Liu et al., 2019).

Traditional statistical methods often fall short when dealing with the intricacies of geochemical distributions. In contrast, fractal methods reveal underlying patterns consistent across different scales, making them particularly useful for resource exploration, environmental monitoring, and understanding geological processes. By leveraging the fractal nature of geological formations and mineral deposits, researchers can more effectively identify and characterize geochemical anomalies, enhancing exploration efforts' efficiency and accuracy. Fractal methods used in geochemistry include the Concentration-Area (C-A) fractal model, Concentration-Number (C-N) fractal model, Power Spectrum-Area (S-A) fractal model, multifractal modeling, and box-counting fractal dimension. Each method offers unique advantages in separating anomalies from background levels, demonstrating fractal analysis's transformative impact on geochemical research (Afzal et al., 2013; Zue & Wang, 2016; Barak et al., 2018, 2021, 2023, 2024; Sadeghi, 2021; Ghasemi et al., 2024).

Aliyari et al. (2020) proposed a developed zonality index for Cu–Mo porphyry deposits using staged factor analysis in conjunction with the Number-Size (N–S) fractal model, applying this approach to the Serenu deposit in SE Iran. The study highlighted the potential of a zonality index derived from major and minor ore elements to enhance the identification of mineralized zones, suggesting broader applications for other mineralization types.

Building on this, Pougholam et al. (2024) focused on detecting Rare Earth Element (REE) geochemical anomalies associated with Iron-Apatite ores using a deep learning-based image fusion technique. This approach, combined with a wavelet-number (W-N) fractal model, enabled the identification of significant REE anomalies in the Tarom region, NW Iran, underscoring the utility of fractal-wavelet modeling in delineating ore deposits.

Heidari et al. (2024) investigated the differentiation between Cu-Mo and Cu-Au porphyry deposits within the Urumieh-Dokhtar magmatic arc in Iran. Utilizing the Mo/Au geochemical index through the Concentration-Number (C-N) fractal model, the study effectively distinguished between these deposit types, revealing a correlation between their distribution and geological periods, with Cu-Mo deposits predominantly forming during the Miocene.

The application of fractal models extends beyond mineral exploration to oil and gas reservoir studies. Afzal et al. (2023) employed concentration-area (C-A) and concentration-number (C-N) fractal analyses to classify productivity index (PI) zones in a fractured rock reservoir in southern Iran. The findings indicated that areas with higher PI values, linked to fault zones and fractures, demonstrated superior reservoir quality, illustrating the accuracy of multifractal methods in geological modeling.

Moreover, Paravarzar et al. (2023) utilized the Concentration-Volume (C-V) fractal model

and Turning Band Simulation to analyze gold mineralization stages in the Zarshuran Carlin-type gold deposit in NW Iran. The study effectively identified mineralized zones within specific lithological units, emphasizing the relevance of fractal models in characterizing gold deposits.

In this research, exploratory geochemical investigations were conducted on 506 stream sediment samples from the Siah Cheshmeh area in Northwest Iran. Following preprocessing and the calculation of background values using enrichment index studies, univariate, bivariate, and multivariate statistical analyses were performed on the stream sediment data using SPSS software. By employing Exploratory Data Analysis (EDA) and Concentration-Number (C-N) fractal modeling, background populations were separated from anomalies. This allowed the identification of promising areas based on the obtained information and their prioritization for subsequent exploration stages. The main objective of this study is to compare and evaluate the effectiveness of classical statistical methods, Exploratory Data Analysis (EDA), and grade-number fractal modeling in separating anomalies from the background and determining threshold values.

The study area is located within the Khoy ophiolite zone, part of the extensive Tethyan ophiolite belt that stretches across northwest Iran along the Iran-Turkey border. This ophiolitic zone is significant in terms of metallogenesis, featuring various mineralization types. Key mineral resources include podiform chromite (Cr mineralization) associated with serpentinized ultramafic host rocks, Cyprus-type volcanogenic massive sulfide deposits (Cu-Zn ± Au), as well as Mn-Fe mineralization found in pelagic sediments and radiolarian cherts. Additionally, Au-Hg mineralization associated with listwanitic rocks is noteworthy. This research focuses on prospecting these critical mineralization types.

Geological Overview of the Siah Cheshmeh Region

The eastern part of the Siah Cheshmeh map falls within the Alborz-Azerbaijan zone (Nabavi, 1976) or Central Iran (Berberian & King, 1981; Nogole-Sadat & Almasian, 1993). The western part of this region features blocks of metamorphic and ophiolitic rocks with faulted boundaries, adjacent to the sedimentary units of the Central Iran zone. Key rock units in this area include Permian limestones, Mesozoic sediments, Oligocene-Miocene deposits, and Neogene clastic deposits, which appear un-metamorphosed in the east and northeast of the map (Fig. 1).

The Siah Cheshmeh region is part of the northwestern ophiolite belt of Iran, extending from the Anatolian mountains in Turkey eastward, covering an extensive area of approximately 3900 square kilometers along the Iran-Turkey border. This ophiolite sequence includes ultramafic rocks, mafic rocks, diabase dikes, and sedimentary rocks (limestones, pelagic shales, radiolarian cherts, and flysch). Notably, sedimentary rocks extend further north and predominantly appear as mélanges.

At the highest levels of the ophiolite sequence, and associated with radiolarian cherts, jasperoids, and pelagic limestones, manganese deposits manifest in various forms, including lenticular, framework, massive, and banded structures. Similar deposits are noted in other ophiolitic regions of Iran, such as Chah Bashi (south of Na'in), Nabuyd and Salm Rud (Sabzevar ophiolitic mélange), Konich (Iranshahr ophiolite), and mineral indications in the Tashk region (Fars province). The reserves of these deposits generally range from a few thousand tons, with the Chah Bashi deposit estimated to contain 10.3 million tons (Imamalipour, 2009). In the Khoy ophiolite, indications of similar mineralization, typically in the form of manganese, manganese-iron, iron, and manganese-iron-copper deposits, are found, with notable examples including Aghbolagh and Aghbash (northwest of Khoy), Dilk Vardi, and Safo (north of Chaldoran). These deposits are part of the sedimentary sections of the Khoy ophiolite complex and exhibit significant tectonic mixing with ophiolitic rocks, resulting in mélange formations (Imamalipour, 2009).

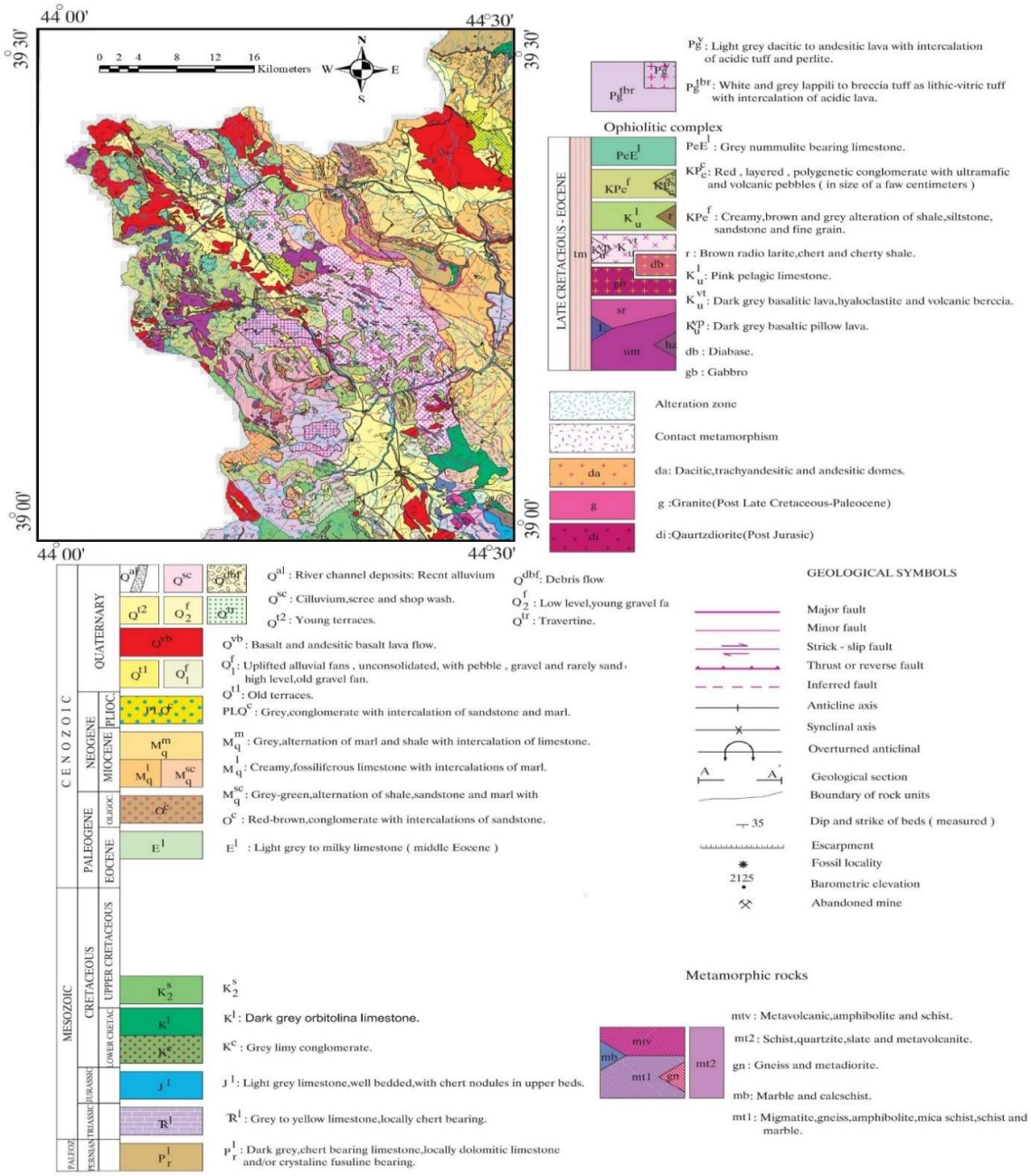

Figure 1. the 1:100,000 geological map of study area (Imamalipour, 2009)

Based on the structural position, the studied area can be divided into three sections (Majidi & Ghalamghash, 2004): 1. the southwestern margin of the Central Iran zone, 2. the metamorphic rock complex, and 3. the ophiolite complex and associated rocks.

Igneous rocks, including Mesozoic intrusive rocks and Paleogene volcanic and quartzitic rocks, are also exposed in the region. The metamorphic and ophiolite rock complexes appear to be part of the northwestern extension of the Sanandaj-Sirjan zone, which outcrops in the southwestern part of the studied area. The 1:100,000 geological map of the study area (Fig. 1) provides detailed geological information, including the distribution of various rock types, structural features, and mineral deposits, serving as a crucial tool for understanding the geological setting and guiding geochemical investigations.

In Central Iran, the oldest rock units date back to the Permian and Triassic periods. The lower

boundary of the Permian carbonate rocks is either faulted or covered. Based on the lithology of the Ruteh Formation, shallow marine conditions are inferred for their formation. The contacts between the Permian and Triassic units and the Triassic-Jurassic units are not visible, complicating the interpretation of events between these periods. However, marine conditions prevailed during the Triassic and Jurassic periods, as evidenced by carbonate rocks and fossils.

In the southeastern part of the region, Jurassic carbonate rocks are conformably overlain by clastic units and Orbitolina-bearing limestones of the Early Cretaceous. This indicates a marine regression and emergence in the late Jurassic. At the beginning of the Cretaceous, marine conditions resumed until the end of the period. Early Cretaceous carbonate rocks are unconformably overlain by Oligocene or Miocene clastic units, suggesting uplift by orogenic movements at the end of the Early Cretaceous, with continental conditions prevailing until the Miocene. In the Miocene, marine conditions returned, persisting until the early Miocene.

Sampling Network Design and Field Survey in the Siah Cheshmeh

Before designing the sampling network, it is essential to review all available information, including the geological characteristics of the area, fault data, topographic conditions, and previous geochemical and heavy mineral survey results. This preliminary analysis ensures that the sampling network is optimally designed to identify and differentiate geochemical anomalies related to mineral deposits from other types of anomalies.

To accurately detect true geochemical anomalies and differentiate those related to mineral deposits from other sources, a consistent fraction of stream sediments must be tested. This involves examining sediments with a mesh size of 80 for silt and 20 for heavy minerals. The size of the constant fraction is influenced by local climatic conditions, topography, and the distance from the mineralization source.

In regional geochemical surveys, river sediments provide the best sampling sites due to their response to varying climatic conditions, geological settings, topography, mineralization, and stream and regional slopes. Generally, the density of sampling is determined by the drainage density within the basin. For mountainous temperate regions like the study area, a sampling density of one sample per two to three square kilometers is considered adequate.

Considering the outcrop areas, fault lines, significant geological contacts, areas with high fault density, concealed faults, and agricultural, industrial, and military zones surrounding the study area, a total of 506 samples were collected. This sampling was guided by the geochemical map shown in Fig. 2, which ensures comprehensive coverage of the area. The key consideration for sampling is as follow:

Geological Features: Detailed knowledge of the geology, including rock types and structures, to target potential mineralized zones.

Faults and Contacts: Mapping and sampling near faults and geological contacts, as these are often associated with mineralization.

Topography: Understanding the terrain to identify suitable sampling points and ensure safety and accessibility.

Anomaly Identification: Previous geochemical anomalies guide the focus areas for sampling to validate and refine anomaly detection.

Environmental and Land Use: Considering land use patterns, such as agricultural, industrial, and military areas, to avoid sampling bias and ensure representative samples.

This comprehensive approach ensures that the sampling network is scientifically robust, providing reliable data for identifying and analyzing geochemical anomalies in the study area.

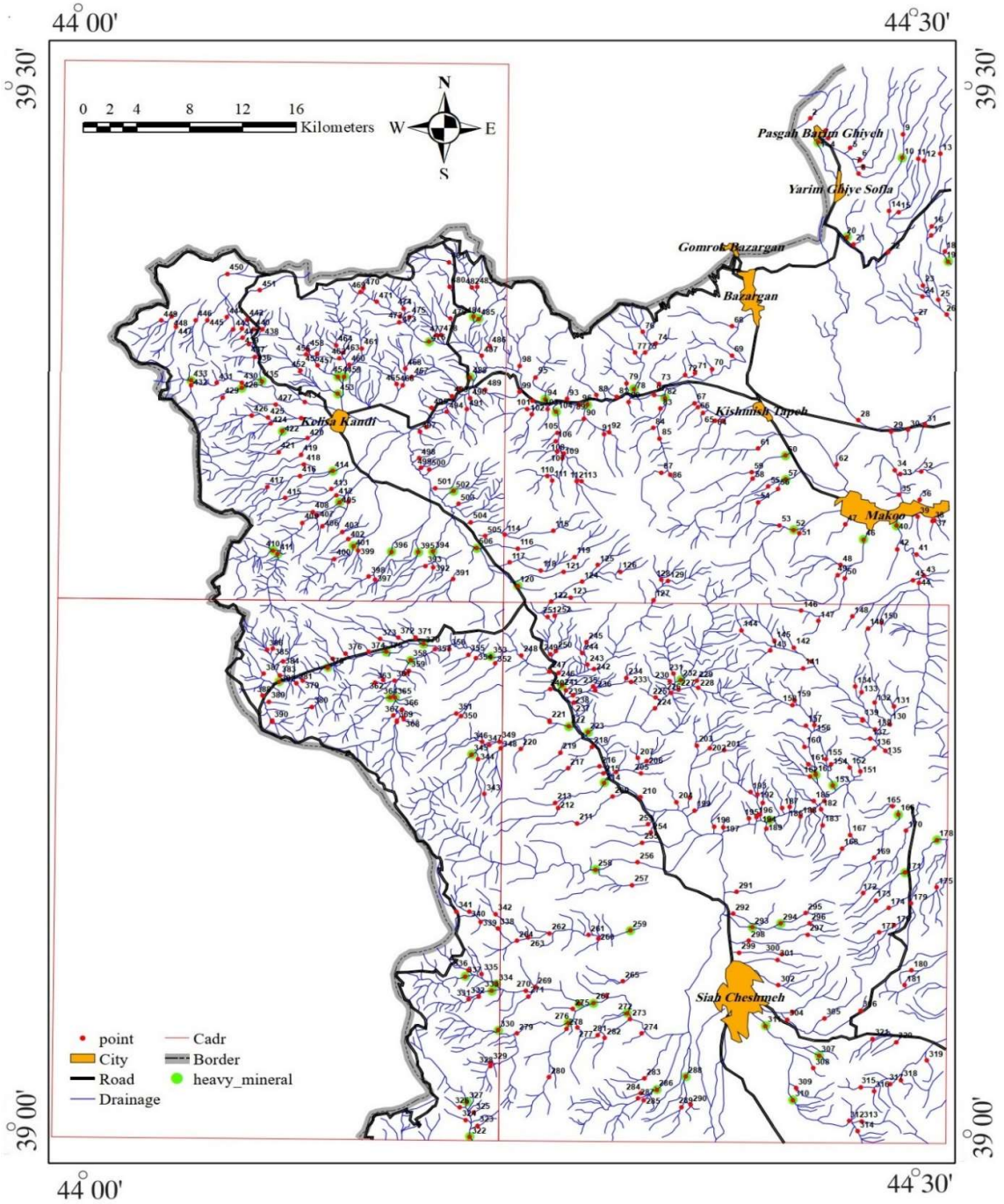

Figure 2. The map showing the spatial distribution of stream sediment samples collected in the 1:100,000 scale Siah Cheshmeh sheet

Preprocessing of raw data

Before the geochemical data analysis, a series of studies known as preprocessing are conducted, which were also applied to the Siah Cheshmeh data.

In this study area, values greater than the upper sensitivity limit are replaced with 3/4 of the upper sensitivity limit, and values less than the lower sensitivity limit are replaced with 4/3 of that limit. This approach is typically employed when the number of censored sensor data points (less than 10% of total data) is minimal. A major drawback of this method is that it is not

influenced by the statistical parameters of the data population and solely functions based on the sensitivity limit measurement function (Hassani-Pak & Sharafaddin, 2002). In Table 1, the count of each element's sensitivity and the laboratory-reported measurements for all elements are provided. All elements are reported in ppm, and only gold is reported in ppb.

Subsequently, histograms and cumulative distribution function plots were created for all raw data using Excel 2022 software, these diagrams were shown in Fig. 3a, b for gold element. Then, univariate statistical analyses were conducted using SPSS version 21 software to extract statistical parameters including mean, standard deviation, variance, skewness, kurtosis, maximum, minimum, and other relevant measures (Table. 2).

Given the necessity of identifying outliers in the element distribution function and subsequently correcting or removing them, the data underwent a thorough examination. Considering that removing these values is not permissible, especially for high-grade values due to the potential loss of anomalous areas, the outliers were replaced with appropriate values derived from the Doerffel method based on the number of samples at a 99% confidence level (Hassani-Pak & Sharafaddin, 2002).

Based on Table 3, and the comparison of the concentration of several elements in the study area with the global concentration of elements (Barbalace, 2007), it is observed that the concentration of some elements in the study area is richer compared to the global average.

Table 1. The number and approximate values of sensitivity for each variable

Element	approximate values of sensitivity	Number	Element	approximate values of sensitivity	Number
Ag	0.03	0	**Nb**	5.79	0
Al	3.70	0	**Ni**	16	0
As	1.69	0	**P**	0.05	0
Au	1.00	49	**Pb**	0.93	0
Ba	38.60	0	**Rb**	-2.55	0
Be	0.23	0	**S**	0.03	0
Bi	0.08	123	**Sb**	0.30	0
Ca	6.60	0	**Sc**	3.45	0
Cd	0.08	30	**Se**	0.08	6
Ce	5.87	0	**Sn**	0.2	3
Co	2.10	0	**Sr**	56.8	0
Cr	22.00	0	**Te**	0.01	0
Cs	0.87	0	**Th**	2.78	0
Cu	8.31	0	**Ti**	0.27	0
Fe	2.40	0	**Tl**	0.03	0
Hg	0.04	259	**U**	0.75	14
K	0.50	0	**V**	28.46	0
La	5.08	1	**W**	0.32	0
Li	7.26	0	**Y**	6.33	0
Mg	1.2	0	**Yb**	1.23	0
Mn	0.04	0	**Zn**	18.52	0
Mo	0.2	0	**Zr**	75	0
Na	0.8	0			

Table 2. Descriptive statistics of data under assessment

Elements	Ag	Au	Ba	Cr	Cu	Fe
Mean	0.12	1.98	302.87	412.59	45.73	62709.79
Median	0.08	1.7	277.37	277.53	42.47	67043.55
Std. Deviation	0.08	1.44	166.26	354.32	21.3	22154.76
Variance	0.01	2.09	27640.94	125539.67	453.86	490833539
Skewness	3.91	8.17	2.18	1.27	0.63	-0.49
Kurtosis	28.1	109.65	9.04	0.85	0.34	0.49
Range	0.88	23	1296.97	1789.49	117.23	153969.39
Minimum	0.03	1	38.64	21.82	8.31	2.37
Maximum	0.91	24	1335.61	1811.31	125.54	153971.77
Elements	**Hg**	**Mn**	**Ni**	**Pb**	**S**	**Zn**
Mean	0.26	1044	289.65	14.43	521.69	70.17
Median	0.04	1064.9	145.84	12.08	386.38	69.27
Std. Deviation	1.25	420.11	296.51	17.99	526.88	30.86
Variance	1.56	176495.13	87918.42	323.69	277607.4	952.15
Skewness	9.74	0.3	1.58	15.51	4.85	10.54
Kurtosis	111.64	1.22	2.23	298.21	35.37	175.33
Range	17.95	2619.2	1743.51	367.27	5667.48	582.96
Minimum	0.04	0.05	15.54	0.93	0.03	18.52
Maximum	17.99	2619.25	1759.05	368.2	5667.51	601.48

Table 3. The table illustrates the comparison between the average concentrations of various elements in the study area and their respective global average concentrations

Element	Ag	Au	Ba	Cr	Cu	Fe	Hg	Mn	Ni	Pb	S	Zn
Average of global concentration	0.07	0.0011	340	100	50	41000	0.05	950	80	14.000	260	70
Average of study area concentration	0.12	1.984	410	413	65.73	62710	0.26	1044	290	14.425	522	70.17

Estimate the Background Levels

After homogenizing various populations, the geochemical samples taken from stream sediments were used to calculate the background levels based on the type of upstream rock or rocks. In this context, the average value was selected as the background level. Each element's value in each sample from a population was then divided by the average value of that element in the population to calculate the enrichment or depletion ratio for that element in each sample. Naturally, elements with a ratio greater than one are considered enriched, while those with a ratio less than one are considered depleted (Hassani-Pak & Sharafaddin, 2002).

The Enrichment Index (EI), which eliminates the effect of upstream rock for a specific element in a given sample, is defined as the ratio of the concentration of that element in the sample to the average concentration of the same element in the population to which the sample belongs. Thus, the factors influencing the Enrichment Index of a specific element in a particular sample depend not only on the amount of that element in the sample but also on the abundance of that element in the associated population.

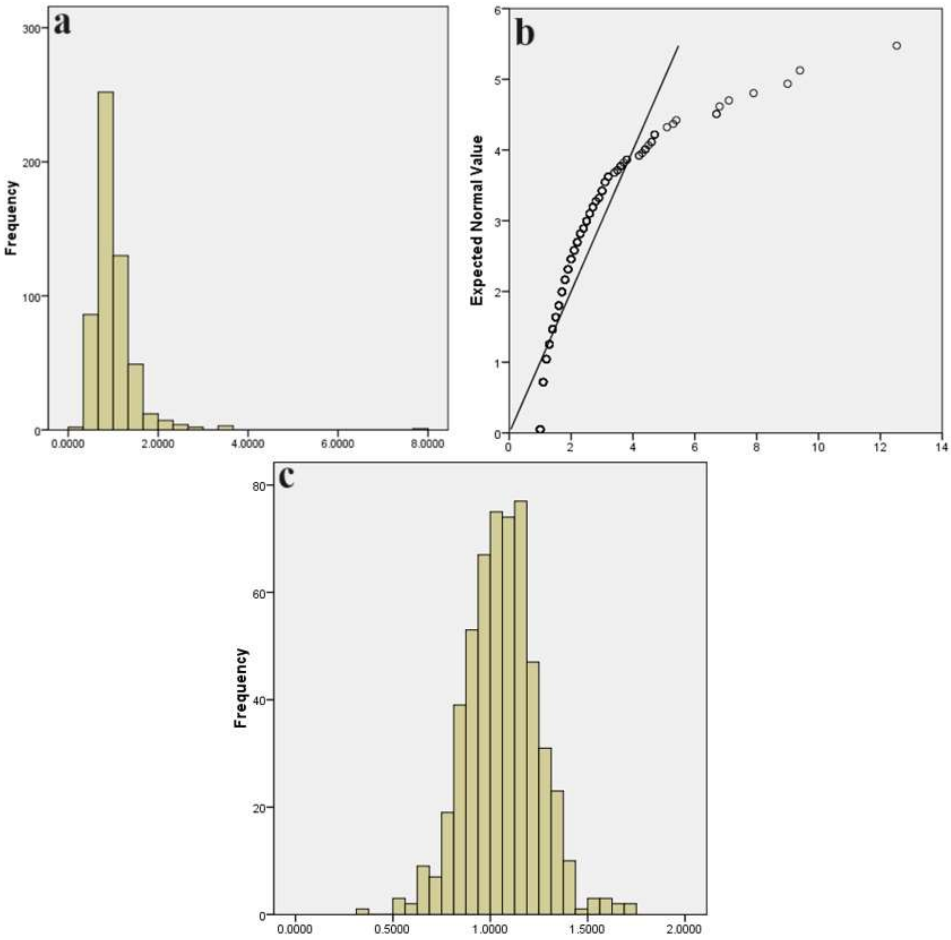

Figure 3. histogram (a) and cumulative distribution (b), and the normalized histogram (c) for gold element.

Therefore, if the local and regional abundance of an element both increase or decrease at a constant rate, the Enrichment Index remains constant because both the numerator and denominator of the ratio increase or decrease proportionally. Consequently, the Enrichment Index is relatively independent of the lithological factor or the syngenetic component of an element's abundance in the source area of stream sediments. Since the Enrichment Index can render geochemical data independent of lithological changes (syngenetic component) in the source area, it has been used as the basis for calculations in this study. The equation below is used to calculate the single-element Enrichment Index in each sample:

$$E_i = \frac{C_i}{C_m}$$

where Ci is the concentration of the element in the sample and Cm is the average concentration of the element in the population. After normalizing each element's value in each population by dividing it by the average value of the same element in the same population (thus normalizing for the effects of different lithologies), it becomes possible to combine the results from samples belonging to various populations into a comprehensive population. Statistical analysis can then be conducted on this comprehensive population. Since the results from the previous phase represent the Enrichment Index (EI) of each element, the comprehensive population obtained is referred to as the Enrichment Index population. With careful attention to the geological map, this population can be largely independent of the lithological factors in the source area of the stream sediments (Hassani-Pak & Sharafaddin, 2002). Subsequent processing and analyses in

this study have been performed on the Enrichment Index values.

To normalize the data, the Cox-Box algorithm was implemented using S-Gems and Minitab software, the normalized diagram of gold element was shown in Fig. 3c.

Multi-variate calculations and statistical processes

Multivariate calculations and statistical processes in geochemistry involve analyzing multiple variables simultaneously to understand complex relationships between geochemical data. These methods help to identify patterns, anomalies, and correlations among different elements or compounds in geological samples.

The Pearson correlation coefficient is a parametric method used for data with a normal distribution or a large number of data points. When the assumption of normality is not reasonable, the Spearman correlation coefficient is used instead. This method is not based on the actual values but is calculated based on the ranks of the data (Momeni & Faal-Qayoumi, 2012).

Correlation matrices have been calculated using raw data and data adjusted with the enrichment index using the Pearson method. The results of these calculations are presented in Table 4. According to this table, the elements chromium and nickel have the highest correlation with a coefficient of 0.88.

Factor analysis is based on eigenvectors, where eigenvalues and eigenvectors are used to identify directions with maximum variability. By defining new variables that are linear combinations of the original variables, the number of dimensions (variables) is reduced, and the contribution of each variable to the variability is determined. This feature (reducing the number of dimensions or variables) may not be very significant for a two-dimensional space, but its advantage becomes evident when considering a 39-dimensional (elemental) space and reducing it to 10 dimensions. This reduction is highly important in terms of data visualization, understanding variability, and computational efficiency (Hassani-Pak & Sharafaddin, 2002).

Yousefi et al. (2014, 2023) highlighted that factor analysis outcomes are highly sensitive to geochemical noise, largely due to the mathematical limitations of the method itself. To address this issue and to better detect distinct anomalous geochemical patterns, they introduced the concept of staged factor analysis (SFA). This innovative approach involves systematically excluding non-indicator elements from the analysis, resulting in a clearer, more coherent multi-element geochemical signature with minimized noise (Yousefi et al., 2014, 2023).

Table 4. Pearson correlation coefficients for 12 items

	Ag	Au	Ba	Cr	Cu	Fe	Hg	Mn	Ni	Pb	S	Zn
Ag	1.00											
Au	-0.02	1.00										
Ba	0.13	0.11	1.00									
Cr	-0.12	0.23	-0.26	1.00								
Cu	0.20	0.35	0.10	0.28	1.00							
Fe	-0.04	0.13	-0.05	0.15	-0.08	1.00						
Hg	0.07	-0.03	0.01	0.07	0.28	-0.46	1.00					
Mn	0.06	0.33	-0.04	0.21	0.35	0.42	-0.15	1.00				
Ni	-0.13	0.23	-0.34	0.89	0.23	0.16	0.04	0.38	1.00			
Pb	0.34	0.05	0.43	-0.34	0.09	-0.09	0.03	-0.06	-0.29	1.00		
S	0.12	-0.06	0.20	-0.35	-0.12	-0.08	-0.03	0.08	-0.22	0.20	1.00	
Zn	0.31	0.14	0.23	0.16	0.46	0.13	0.08	0.23	0.09	0.27	-0.03	1.00

The SFA method allows for the derivation of reliable factor scores, which can then be used to identify samples with high factor scores as indicators of specific mineral deposit types, guided by established geochemical criteria. As a multivariate analytical technique, SFA effectively reduces the number of geochemical variables while simultaneously revealing interrelationships among these variables (Carranza & Hale, 1997). This methodology was applied to SR data to investigate the associations between trace elements in the study area, enhancing the understanding of geochemical processes in the context of mineral exploration. Table 5 (in this table, values exceeding the 0.57 have been highlighted in bold.**)** shows the rotated matrix of factor analysis in the Siah Cheshameh area. The outcomes of the SFA method in the final stage revealed the presence of five distinct groups in the area. Factor 1 (Fac1) comprises elements including Al, Au, Be, Ce, Cs, K, La, Nb, P, Ti, Y, Yb, and Zr. Factor 2 (Fac2) encompasses Ba, Ca, Co, Cr, Cu, Fe, Mg, Mn, Ni, Sr, and Zn. Factor 3 (Fac3) includes Hg, S, Th, and U. Factor 4 (Fac4) consists of Bi and Pb, while Factor 5 (Fac5) contains As, Cd, and W.

Table 5. The rotated component's matrices with variamax rotation in the Siah Cheshameh area

	Stage 1						Stage 2				
Ele.	**Fac1**	**Fac2**	**Fact3**	**Fac4**	**Fact5**	**Ele.**	**Fac1**	**Fac2**	**Fact3**	**Fac4**	**Fact5**
Ag	0.382	0.13	0.028	0.444	0.103	**Al**	**0.806**	0.256	0.275	-0.191	-0.08
Al	**0.8**	0.302	-0.283	-0.048	0.143	**As**	-0.011	-0.233	0.082	-0.176	**0.798**
As	0.005	-0.246	-0.045	**0.808**	0.131	**Au**	**0.592**	-0.012	0.064	-0.266	-0.095
Au	-0.032	**0.579**	-0.054	-0.124	0.28	**Ba**	-0.238	**0.601**	-0.015	-0.377	-0.134
Ba	**0.628**	-0.205	0.043	-0.138	0.339	**Be**	**0.888**	-0.168	-0.077	-0.168	0.124
Be	**0.903**	-0.126	0.073	0.118	0.137	**Bi**	0.036	-0.045	0.079	**-0.816**	0.093
Bi	0.08	-0.046	-0.061	0.128	**0.795**	**Ca**	-0.154	**-0.725**	0.442	0.181	0.088
Ca	-0.122	**-0.739**	-0.421	0.058	-0.199	**Cd**	0.161	-0.34	0.023	-0.011	**0.786**
Cd	0.183	-0.337	-0.014	**0.759**	-0.062	**Ce**	**0.888**	-0.231	-0.227	-0.065	0.01
Ce	**0.898**	-0.187	0.234	-0.013	0.031	**Co**	-0.148	**0.782**	-0.222	0.291	0.2
Co	-0.202	**0.772**	0.194	0.171	-0.279	**Cr**	-0.391	**0.782**	-0.113	0.215	-0.159
Cr	-0.443	**0.759**	0.098	-0.176	-0.173	**Cs**	**0.688**	0.081	-0.467	0.069	-0.032
Cs	**0.683**	0.132	0.459	-0.039	-0.13	**Cu**	0.414	**0.574**	-0.13	0.035	-0.085
Cu	0.383	**0.61**	0.137	-0.06	-0.092	**Fe**	0.27	**0.846**	0.226	0.162	-0.158
Fe	0.215	**0.854**	-0.241	-0.171	-0.161	**Hg**	-0.089	-0.167	**-0.646**	-0.178	0.06
Hg	-0.067	-0.148	**0.645**	0.093	0.138	**K**	**0.809**	-0.201	0.276	-0.124	0.033
K	**0.822**	-0.167	-0.267	0.035	0.106	**La**	**0.8**	-0.349	-0.055	0.165	0.117
La	**0.804**	-0.308	0.055	0.106	-0.199	**Mg**	-0.391	**0.752**	0.254	0.313	-0.098
Mg	-0.449	**0.726**	-0.276	-0.096	-0.27	**Mn**	0.307	**0.725**	0.263	-0.081	-0.078
Mn	0.266	**0.735**	-0.261	-0.062	0.063	**Nb**	**0.847**	0.107	-0.042	0.199	0.04
Mo	0.497	-0.331	-0.121	0.346	0.281	**Ni**	-0.534	**0.741**	-0.051	0.086	-0.133
Nb	**0.825**	0.145	0.029	0.012	-0.214	**P**	**0.765**	0.008	0.194	0.336	0.14
Ni	-0.579	**0.708**	0.037	-0.135	-0.035	**Pb**	0.364	-0.059	-0.175	**-0.74**	0.235

P	**0.745**	0.044	-0.194	0.099	-0.387	**S**	0.038	-0.067	**0.903**	-0.133	0.179
Pb	0.412	-0.036	0.174	0.253	**0.69**	**Sr**	0.124	**-0.761**	0.157	0.046	-0.027
Rb	0.56	-0.19	0.061	0.004	0.288	**Th**	0.395	0.465	**-0.732**	-0.057	-0.045
S	0.049	-0.085	**-0.908**	0.187	0.134	**Ti**	**0.776**	0.341	0.151	0.171	-0.065
Sb	0.056	-0.093	0.532	0.544	0.247	**U**	-0.052	0.243	**-0.612**	0.082	0.296
Sn	0.303	-0.097	-0.167	0.188	0.176	**W**	0.363	0.04	-0.259	-0.081	**0.636**
Sr	0.163	**-0.751**	-0.123	-0.05	-0.091	**Y**	**0.938**	0.086	0.003	-0.092	-0.006
Th	0.372	0.501	**0.721**	-0.026	0.037	**Yb**	**0.895**	0.106	-0.176	-0.145	0
Ti	**0.744**	0.388	-0.159	-0.057	-0.23	**Zn**	0.535	**0.64**	-0.159	-0.191	0.138
U	-0.061	0.238	**0.595**	0.222	-0.087	**Zr**	**0.911**	0.046	0.137	-0.021	0.057
V	0.556	0.584	0.206	-0.092	-0.302						
W	0.36	0.052	0.258	**0.615**	0.026						
Y	**0.934**	0.137	-0.011	-0.004	0.036						
Yb	**0.894**	0.16	0.165	0.005	0.082						
Zn	0.507	**0.673**	0.146	0.168	0.14						
Zr	**0.903**	0.09	-0.147	0.058	-0.02						

Another multivariate statistical method is cluster analysis. The goal of cluster analysis is to achieve a criterion for classifying variables or samples as appropriately as possible, based on maximum similarity within groups and maximum difference between groups. This feature helps us to classify variables and samples into clusters that have the highest possible internal similarity and the highest possible inter-group differences. The results of cluster analysis are usually displayed in a hierarchical diagram called a dendrogram. This diagram shows how samples or variables are connected to each other. A linear scale is placed at the top of the diagram, and the connection points of each variable to a cluster or one cluster to another on this scale correspond to their degree of similarity (Hassani-Pak & Sharafaddin, 2002; Barak et al., 2020).

In this research, after excluding the elements Li, Na, Sc, Se, Te, and Tl to prevent false similarities in the diagram, the analysis was conducted on thirty-nine elements. The results are shown in Fig. 4.

In group 1, the elements Cr, Ni, Mg, Co, Fe, Mn, and Au are found. This cluster can be divided into two subgroups, including the elements Cr, Ni, Mg, and Co. These elements can be associated with the extension of ultramafic rocks and related mineralizations. Nickel can occur in silicate phases (substituting for magnesium in olivine) or in sulfide phases, requiring exploratory investigation. Chromium can be dispersed in chromite phase within ultramafic rocks and also in mineralization forms (podiform chromite) are conceivable.

The mineralization of Fe and Mn appears in manganese-iron deposits in recognized regions (such as Safow manganese deposit), occurring alongside host rocks of pelitic limestone and radiolarite cherts. Similar mineralization can be expected in other areas, potentially including gold.

In group 2, there are two subgroups. The first subgroup includes Mo, Ag, Pb, and Sn, which due to lithological conditions of the region and placement in an ophiolitic zone, holds less significance. However, the second subgroup consists of Hg, Sb, and As, which could be associated with the extension of listvenitic rocks and their mineralizations.

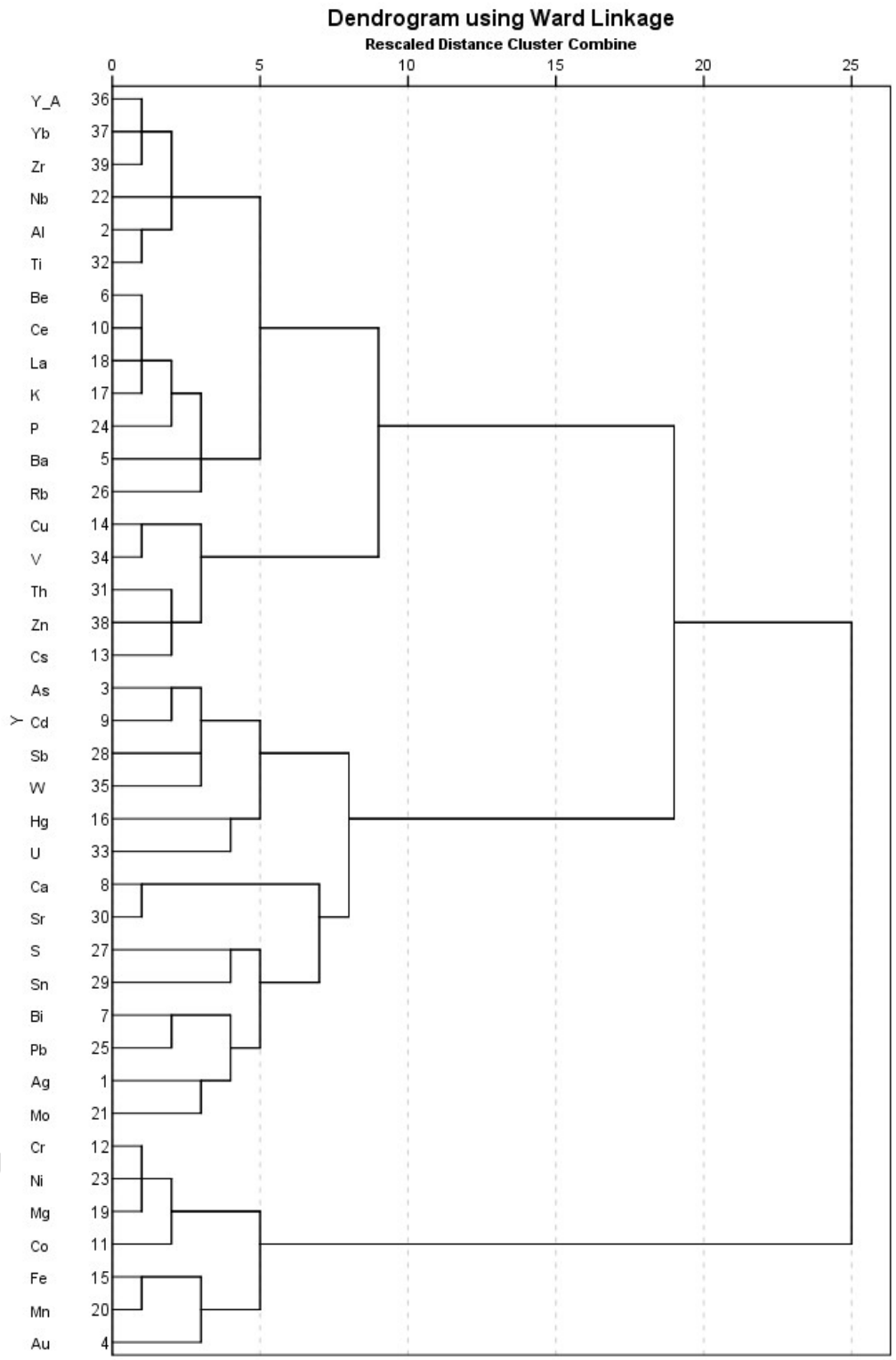

Figure 4. The dendrogram resulting from the cluster analysis for 39 elements

Group 3 includes the elements Zn and Cu, which could indicate concentrations and sulfide mineralizations of Cyprus-type associated with the spread of volcanic basaltic rocks.
Elements in subgroup 4 are likely influenced by lithological effects (rock formation) and are of lesser importance.

Results and discussion

Separation of background values, threshold, and anomalies

In statistical geochemical communities, data distribution often exhibits significant skewness, leading to a log-normal distribution where large values, forming the tail of the distribution, represent anomalies. These values, distinct from the rest of the data (background), delineate prospective areas for economic mineralization. Separating anomalies from background is one of the most crucial stages in geochemical exploration and environmental studies. In other words, distinguishing geochemical patterns into components that can differentiate mineralization-related anomalies from background values resulting from geological processes is the primary objective in ore deposit exploration (Hezarkhani & Seljouqi, 2016).

Before generating anomaly output maps, a zone map was prepared based on the watershed of the upstream samples, as previously mentioned. In regional surveys with alluvial sediment deposits in the upstream watershed, all lithological units contributing sedimentary deposits were identified, which played a role in sample formation. This map is shown in Fig. 5.

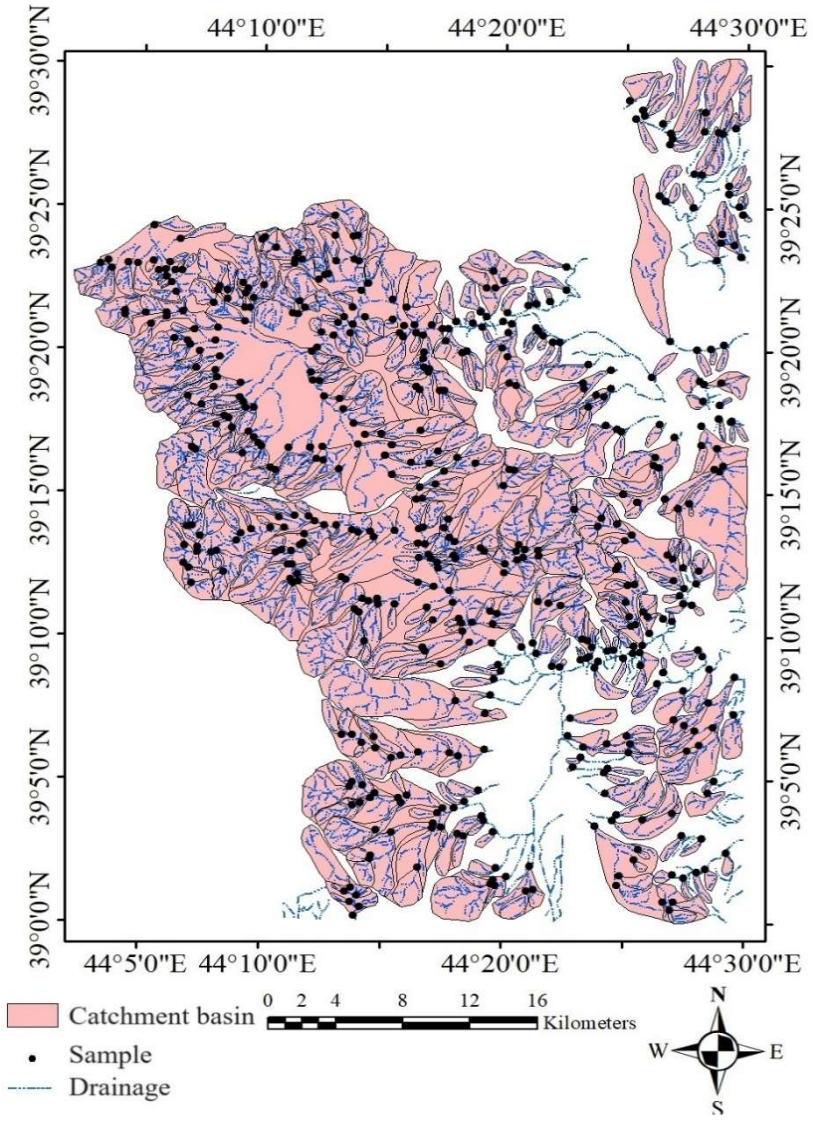

Figure. 5. The catchment basin and drainage of each sample.

Exploratory Data Analysis (EDA)

Exploratory Data Analysis (EDA) is not a method but a robust approach and philosophy in data analysis that includes a set of descriptive statistics and is primarily used as a graphical tool for (Tukey, 1977): (a) Gaining a general understanding of a dataset, (b) Discovering the structure of the data, (c) Defining significant variables in the data, (d) Identifying outliers and anomalies, (e) Formulating and testing hypotheses, (f) Developing cautious models, (g) Identifying the best possible operations and interpreting the data. Thus, classical statistical data analysis and probabilistic data analysis are confirmatory methods based on assumptions about the data distribution model. In contrast, Exploratory Data Analysis, as the name suggests, is an exploratory approach to data analysis.

The aim of Exploratory Data Analysis is to effectively identify data patterns through the strong applications of descriptive statistics and graphical tools, which are qualitatively distinct from classical statistical tools. From a statistical perspective, robust statistics are those that are minimally affected by a few large errors or a large number of small errors (resistance) and are only influenced by a small number of outliers (robustness). The descriptive statistics and graphical tools used in Exploratory Data Analysis are based on the data themselves and their distribution (e.g., normal distribution), while also providing a solid definition of univariate statistics and outliers (Tukey, 1977).

Thresholds can be defined using EDA statistics as Median + 2MAD. In these studies, MAD (Median Absolute Deviation) is defined and calculated using the following formula:

$$MAD = \text{median}(|Xi - \text{median}(X)|)$$

Where: Xi represents the individual data points, and median(X) represents the median of the dataset.

The threshold is then determined by:

$$\text{Threshold} = \text{Median} + 2 \times MAD$$

This method provides a robust measure for identifying outliers and anomalies in the data. The calculations related to this method for the Siyeh Cheshmeh area are shown in Table 6. The anomaly maps of six elements containing Au, Cr, Cu, Fe, Mn, Ni and Zn were created and depicted in Figs. 6a-g.

Fractal Concentration-Number (C-N)

The concentration-number fractal model is based on the inverse relationship between grade and the cumulative frequency of each grade and higher grades. This model has the following general form (Hassanpour & Afzal, 2013):

$$N(\geq \rho) \propto \rho^{-\beta}$$

In this relationship, ρ is the grade of the elements, N is the number of samples containing grades greater than or equal to ρ, and β is the fractal dimension. The main advantage of this method is that it performs calculations before estimation and uses raw, original exploratory data. The breaks between the segments of the straight line on the chart and the corresponding elemental grade values ρ are used as threshold limits for separating geochemical values among various components. These breaks indicate different factors such as lithological differences and geochemical processes (Hassanpour & Afzal, 2013; Barak et al., 2021, 2023). Logarithmic diagrams of the concentration-number (C-N) multifractal models for Au, Cr, Cu, Fe, Mn, Ni and Zn were created and are depicted in Figs. 7a-g. The anomaly maps for these elements are also shown in Figs. 8a-g.

Table 6. Thresholds for elements based on the Exploratory Data Analysis (EDA) method

Element	Au	Cr	Cu	Fe	Mn	Ni	Zn
MEDIAN	-0.05	-0.07	-0.03	-0.02	-0.03	-0.14	-0.014
MAD	0.09	0.20	0.10	0.10	0.10	0.21	0.059
MEDIAN + MAD	0.04	0.14	0.07	0.08	0.07	0.07	0.045
MEDIAN + 2MAD	0.14	0.34	0.17	0.17	0.17	0.28	0.104
MEDIAN + 3MAD	0.23	0.54	0.28	0.27	0.27	0.49	0.162

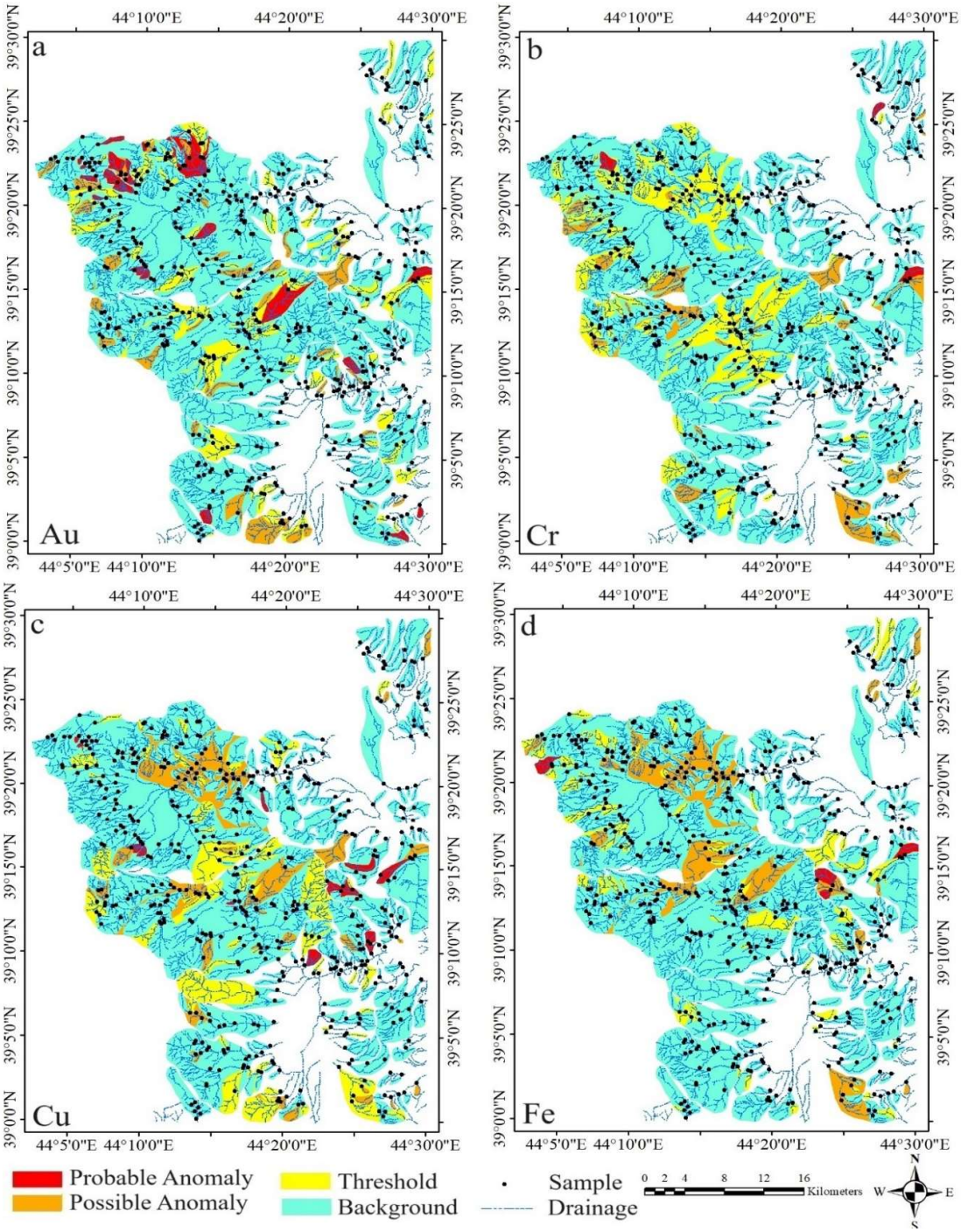

Figure 6. The geochemical threshold map of various elements using the Exploratory Data Analysis (EDA)

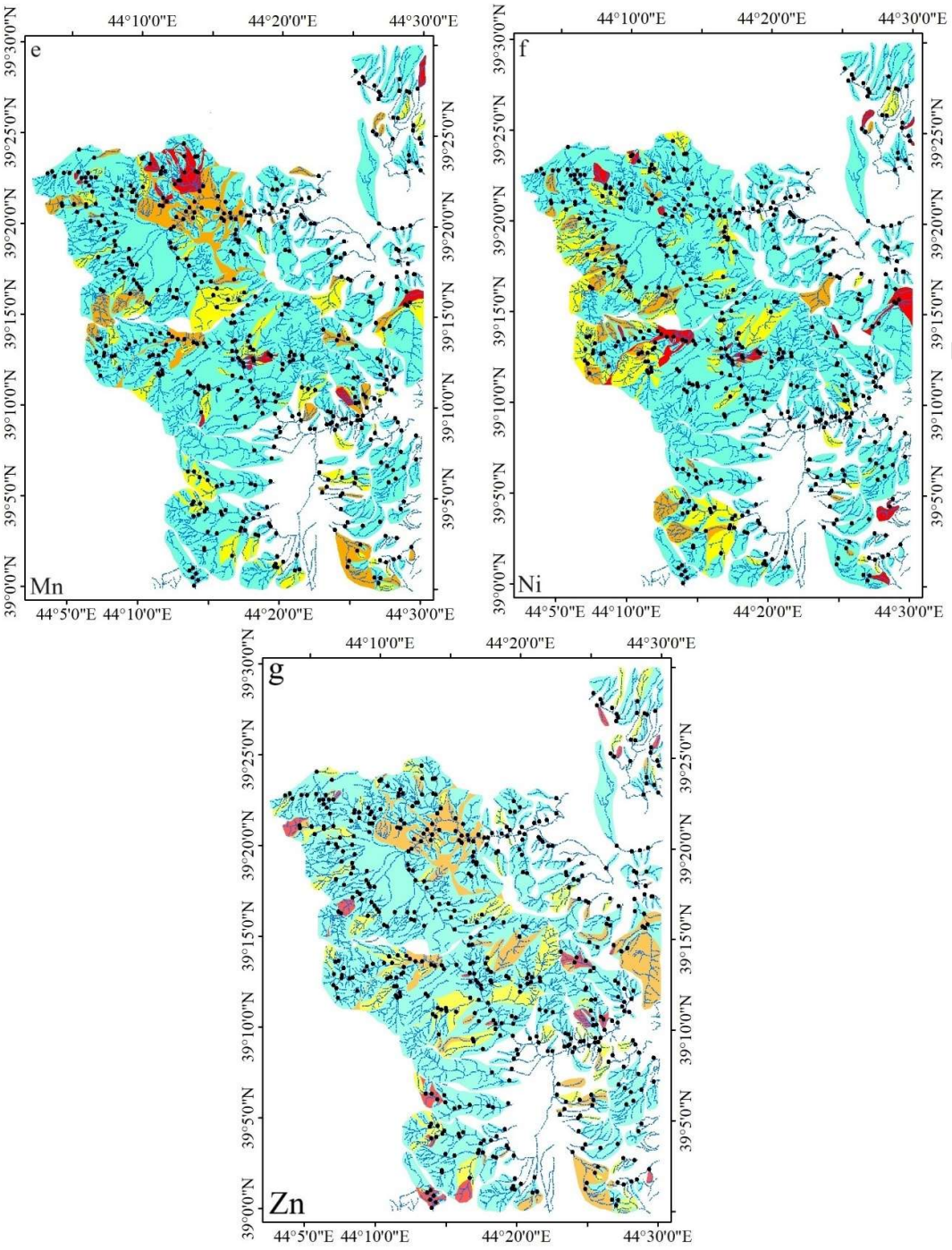

Figure 6. To be continued

Comparison of threshold values obtained from two techniques

Table 7 presents the threshold values calculated for the elements of interest in the study area using both Exploratory Data Analysis (EDA) and concentration-number fractal modeling. The results indicate that the threshold values derived from the fractal method are higher. This suggests that the fractal method performs better in identifying significant thresholds compared to EDA.

Table 7. The threshold values obtained from two techniques

	Au	Cr	Cu	Fe	Mn	Ni	Zn
EDA	2	363.94	70.26	61970	746	696	80.52
Fractal C-N	4.3	136.9	74.72	84135	1384	1061	92.30

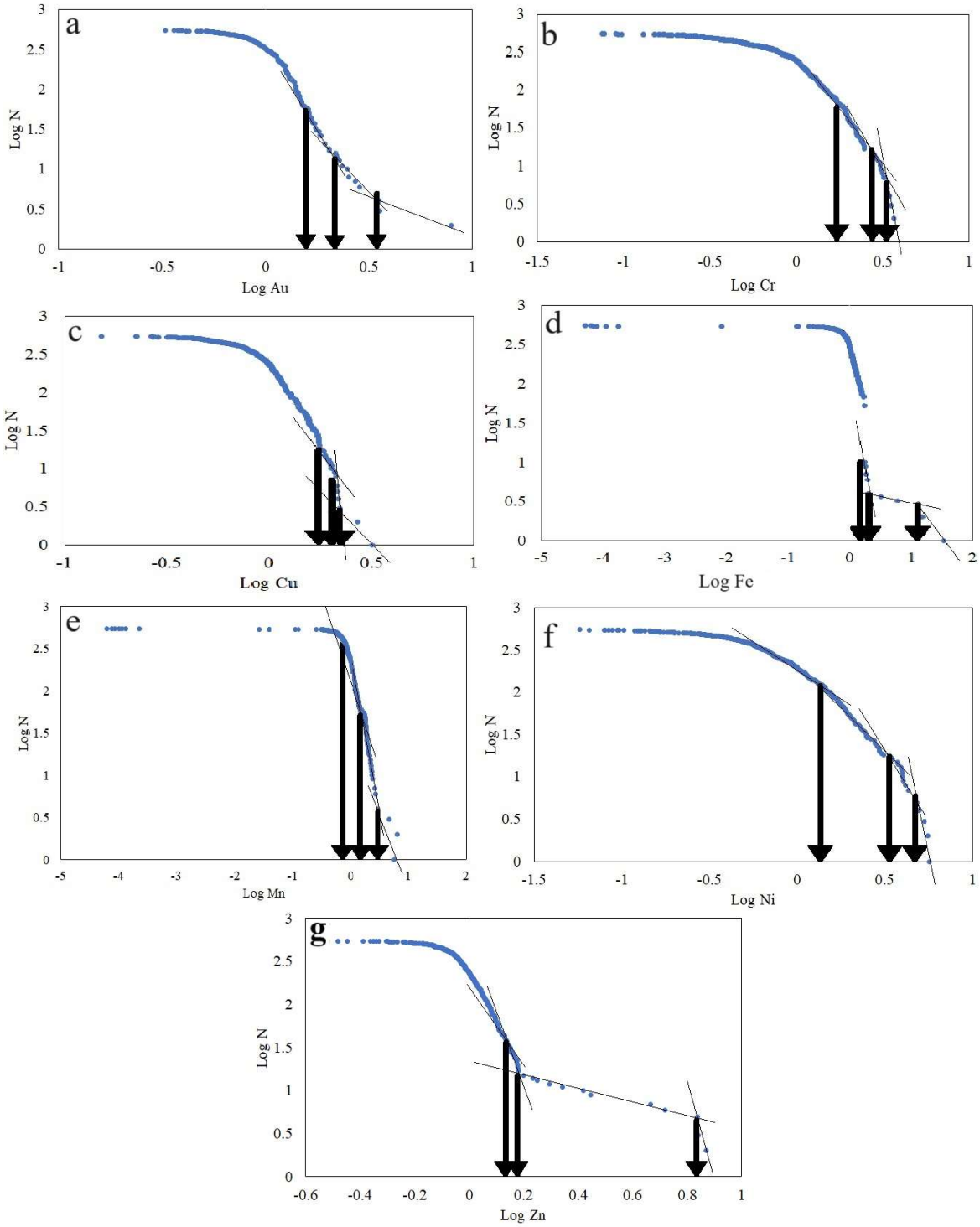

Figure. 7. Logarithmic diagram of the C-N multifractal model for Au (a), Cr (b), Cu (c), Fe (d), Mn (e), Ni (f), Zn (g)

The Comparison of the area of anomalies obtained from two methods

Upon comparing the computed areas using Exploratory Data Analysis (EDA), and concentration-number fractal modeling as outlined in Table 8, the respective totals are 27389655.8 square meters for the fractal method, and 119077065.5 square meters for the EDA method. This comparison leads to the conclusion that the concentration -number fractal modeling method, with the smallest computed area among the approaches, has yielded the most optimal outcome.

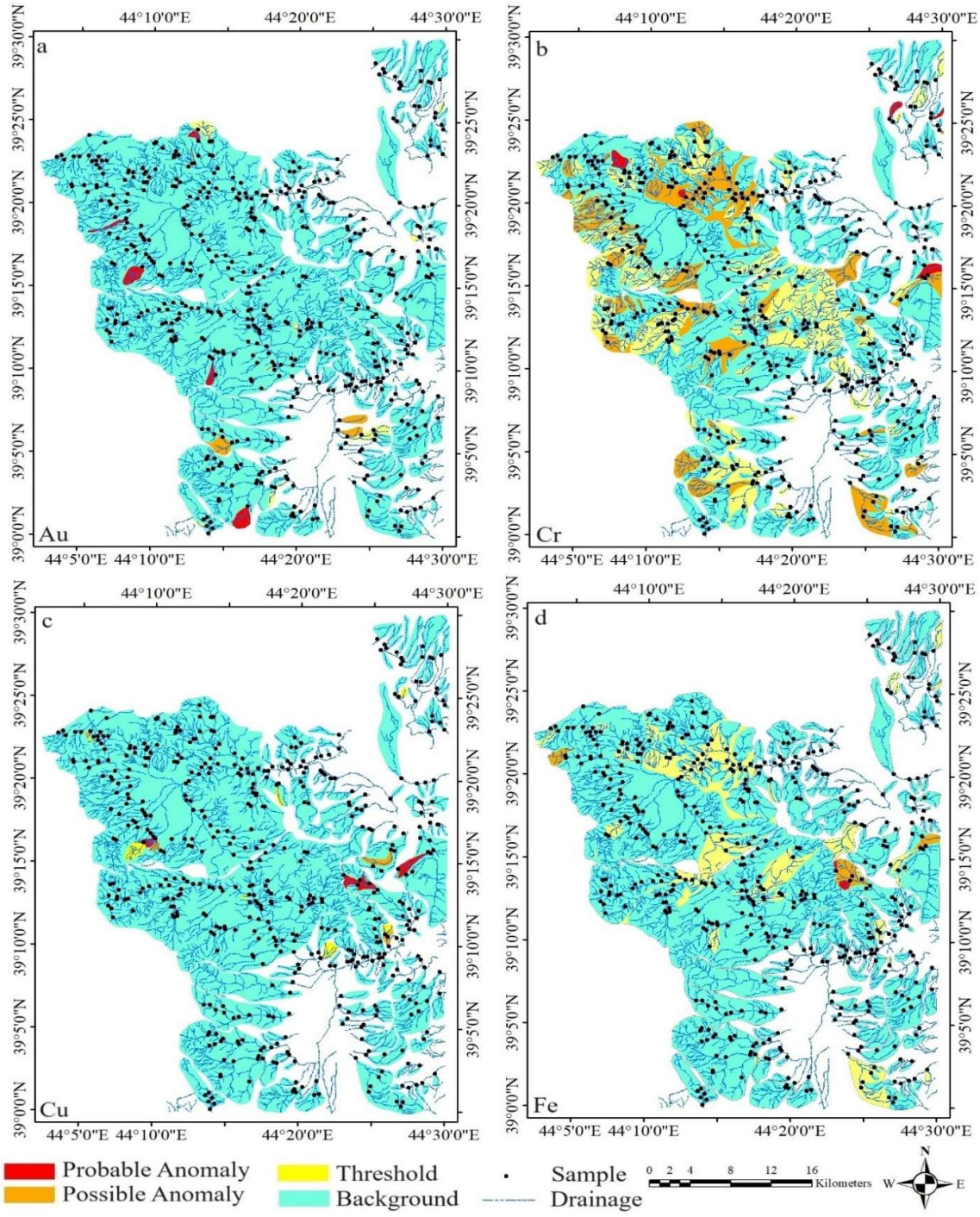

Figure 8. The geochemical threshold map of various elements using the Fractal C-N

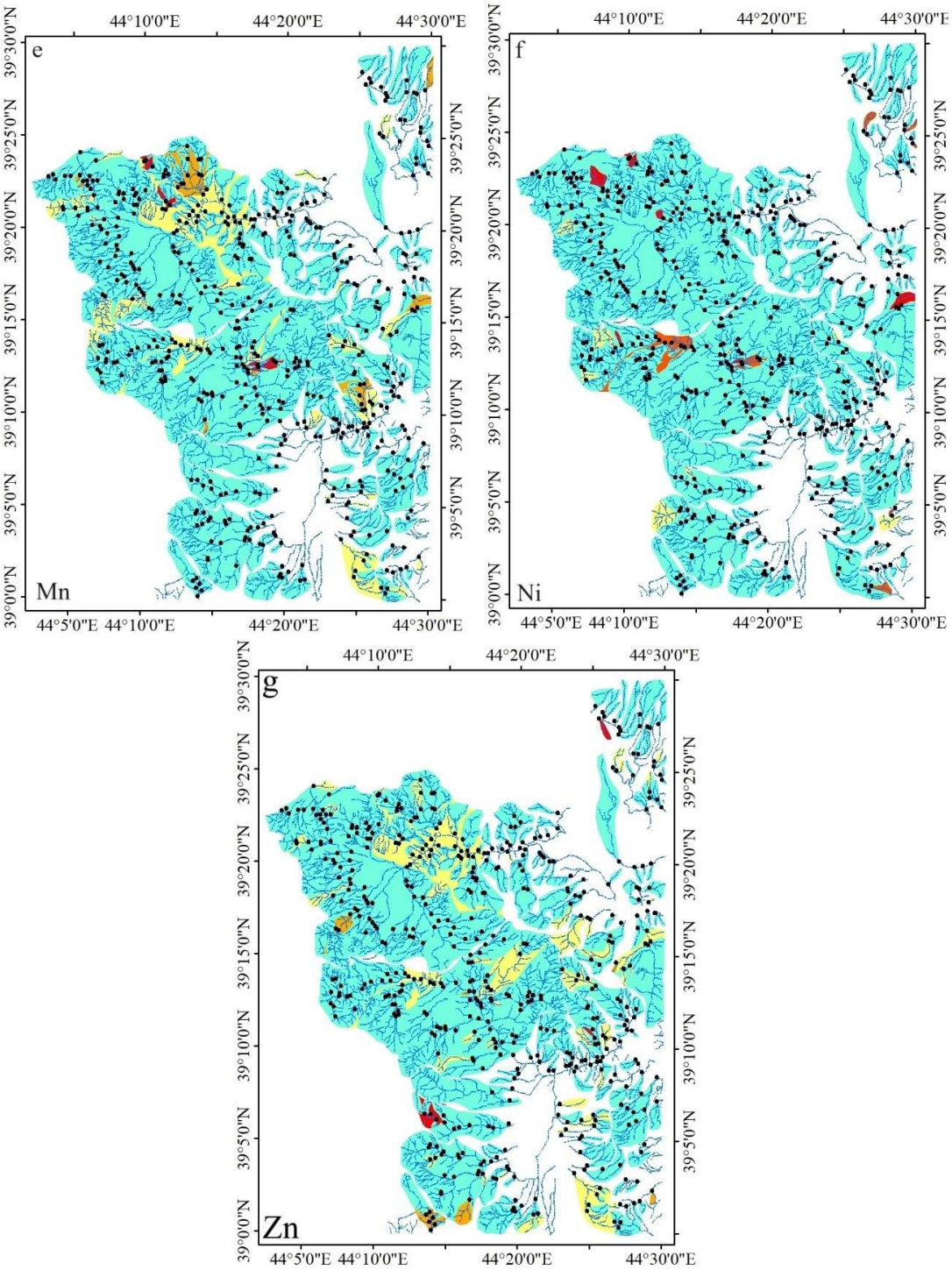

Figure 8. To be continued

Table 8. The area of anomalies values obtained from two techniques

	Au	Cr	Cu	Fe	Mn	Ni	Zn
EDA	41278899.8	5921911.1	14525050.0	8566677.8	22107399.8	26677127.0	25999551.8
Fractal C-N	2115144.6	6957418.3	6419487.7	1184334.4	4551879.2	6161391.6	4531001.6

Therefore, considering that fractal methods take into account the spatial distribution of data and the geometric shape of anomalies, they can be more effective in separating anomalies. Additionally, when comparing the areas of anomalies obtained from EDA methods, the C-N fractal modeling method, with the smallest area, demonstrates the best and most efficient performance compared to classical statistical methods and EDA. Hence, it appears to have better efficiency and performance in anomaly separation. Overall, it can be stated that employing the fractal modeling method in geochemical anomaly separation enhances the accuracy of map preparation, clearly highlighting areas that exceed threshold or anomaly values.

Applying mineralization type analysis in SFA and integration with geochemical mineralization probability index (GMPI)

In this project, GMPI, which was firstly proposed by Yousefi et al. (2012), was used as a mappable weight in MPM. This approach enhances the identification of geochemical anomalies and improves the prediction rate of mineral potential maps, ultimately increasing exploration success. In this section, by eliminating some factors that are not directly related to this type of deposit, not only is the number of factors reduced, but also the areas suitable for this type of deposit are identified. Subsequently, factor analysis was repeated using the key elements of the area (Table. 9).

Using the SFA method, the impact of interfering elements is minimized as much as possible. However, what is more important is the integration of these maps to create a single map that pertains to a specific type of deposit or element, which the GMPI method enables. After calculating the factor scores for the final factors in the previous section, the GMPI values for each factor can be computed, the GMPIs were generated:

$$GMPI_{Au\text{-}Cu\text{-}Fe\text{-}Mn\text{-}Zn} = \frac{e^{Fs_{Au-Cu-Fe-Mn-Z}}}{1+e^{Fs_{Au-Cu-Fe-Mn-Zn}}}$$

$$GMPI_{Cr\text{-}Ni} = \frac{e^{Fs_{Cr-Ni}}}{1+e^{Fs_{Cr-Ni}}}$$

Based on the results shown in Table 7, the GMPI values were calculated for two distinct mineral associations.

The threshold values were determined based on the 95% cumulative frequency for the index components Au, Cr, Cu, Fe, Mn, Ni, and Zn. The threshold was found to be 0.986 for the components Au, Cu, Fe, Mn, and Zn, and 0.729 for the components Cr and Ni. The GMPI values can also be calculated based on cumulative frequency percentages of 99%, 97.5% to highlight anomalies with greater intensity. The results of these calculations are presented in Table 10. Subsequently, the map of prospective exploration areas for the two resulting GMPI values was obtained, as shown in Figs. 9a, b.

Table 9. Rotated matrix of mineralization-influencing elements

Ele.	Fac.1	Fac.2	Fac.3
Au	**0.570**	-0.375	0.154
Cr	0.203	**-0.958**	0.030
Cu	**0.854**	-0.052	-0.083
Fe	**0.702**	-0.448	0.344
Hg	-0.024	0.017	**-0.978**
Mn	**0.829**	-0.243	0.245
Ni	0.111	**-0.975**	0.006
Zn	**0.829**	-0.035	-0.123

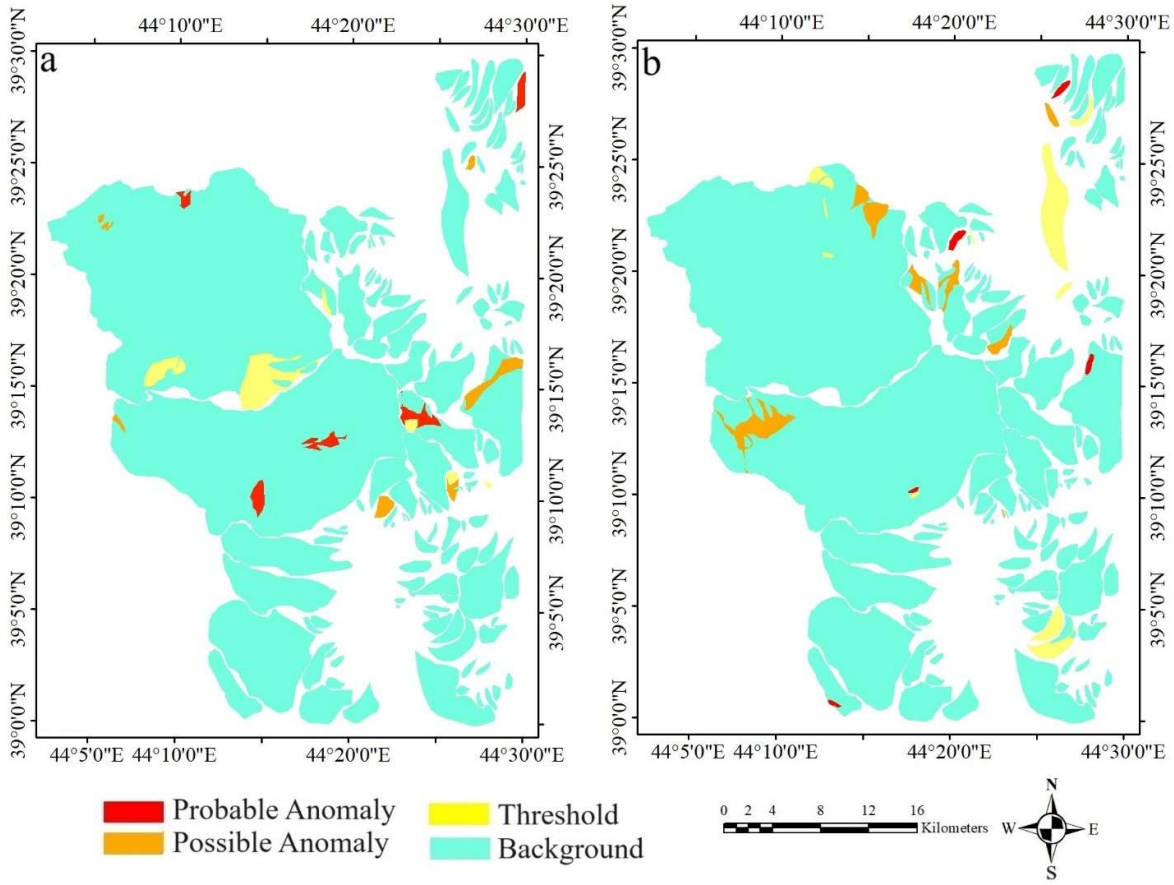

Figure 9. The final MPI maps highlighting areas of high-intensity anomalies

Table 10. The GMPI values of indicator factors based on cumulative frequency percentages of 99%, 97.5%, and 95%

%	$GMPI_{Cr\text{-}Ni}$	$GMPI_{Au\text{-}Cu\text{-}Fe\text{-}Mn\text{-}Zn}$
95	0.729	0.986
97.5	0.772	0.987
99	0.836	0.988

Conclusions

In the northern and northwestern parts of the study area, based on geochemical investigations using both EDA and C-N fractal modeling, anomalies of Au, Ni, Cr, and Mn have been observed, which perfectly align with the analysis provided in the first group of the cluster chart. The mineralization of manganese and iron elements appears as manganese-iron deposits in the region (including the Safow manganese deposit), which occurs alongside pelagic limestone and radiolarian chert host rocks. This type of mineralization can also contain gold. The manganese anomaly zones correspond to the geological units K_u^{vt}, which include hyaloclastite basaltic lava flows and dark gray volcanic breccias from the Eocene, and K_u^{vp}, which consist of dark gray pillow basaltic lavas. With the expansion of ultramafic rocks and associated mineralizations, nickel can occur in the silicate phase by substituting magnesium in olivine, or in the sulfide phase. Chromium can also be present as disseminated chromite within the matrix of ultramafic rocks, or as podiform chromite mineralization. The nickel and chromium anomaly zones align

with the geological units K_u^{vt}, tm (tectonic mélange composed of ophiolite complex rocks), and hz (harzburgite containing olivine plus orthopyroxene) from the Eocene. The gold and silver anomaly zones correspond to the geological units Q^{vb} (basaltic and andesitic-basaltic flows from the Quaternary period) and PeE^1 (light gray nummulitic limestone from the Eocene).

In the western part of the study area, based on geochemical investigations using Exploratory Data Analysis (EDA) and grade-number fractal modeling, copper anomalies have been observed. The presence of pillow basalt outcrops suggests the potential for Cyprus-type copper sulfide mineralization. This region corresponds to the geological units Q^{vb} (basaltic and andesitic-basaltic flows from the Quaternary period) and gb (gabbro from the Eocene).

In the eastern part of the study area, based on geochemical investigations using three methods—classical, Exploratory Data Analysis (EDA), and grade-number fractal modeling-anomalies of iron and copper have been observed. This region corresponds to the geological units R^1 (gray to yellow Triassic limestone and dolomitic limestone, locally cherty) and M_q^m (Miocene alternating marl and shale with interlayers of gray limestone).

By comparing the calculated areas using Exploratory Data Analysis (EDA) and concentration-number fractal modeling, the respective totals are 27,389,655.8 square meters for the fractal method and 119,077,065.5 square meters for the EDA method. This comparison indicates that the concentration-number fractal modeling method, with the smallest calculated area among the approaches, has produced the most optimal result.

The SFA method effectively reduced the influence of interfering elements, leading to the calculation of GMPI values for two distinct mineral associations. The threshold values, based on the 95% cumulative frequency, were identified as 0.986 for Au, Cu, Fe, Mn, and Zn, and 0.729 for Cr and Ni. Additionally, GMPI values were calculated for cumulative frequency percentages of 99% and 97.5% to accentuate higher-intensity anomalies. These results helped in generating exploration maps, highlighting areas with potential for specific types of deposits, thus enhancing the focus on prospective regions for further investigation.

Acknowledgments

This research was made possible with the support of the Office of the Vice-Chancellor for Research and Technology at Urmia University. We gratefully acknowledge their assistance.

References

Afzal, P., Abdideh, M., Daneshvar Saein, L., 2023. Separation of productivity index zones using fractal models to identify promising areas of fractured reservoir rocks. Journal of Petroleum Exploration and Production Technology, 13: 1901-1910.

Aliyari, F., Afzal, P., Lotfi, M., Shokri, S., Feizi, H., 2020. Delineation of geochemical haloes using the developed zonality index model by multivariate and fractal analysis in the Cu–Mo porphyry deposits. Applied Geochemistry, 121: 104694.

Agharezaei, M., Hezarkhani, A., 2016. Delineation of geochemical anomalies based on Cu by the boxplot as an exploratory data analysis (EDA) method and concentration-volume (CV) fractal modeling in Mesgaran mining area, Eastern Iran. Open Journal of Geology, 6: 1269-1278.

Barak, S., Abedi, M., Bahroudi, A., 2020. A knowledge-guided fuzzy inference approach for integrating geophysics, geochemistry, and geology data in a deposit-scale porphyry copper targeting, Saveh, Iran. Bollettino di Geofisica Teorica ed Applicata, 61: 159-176.

Barak, S., Bahroudi, A., Jozanikohan, G., 2018. Exploration of Kahang porphyry copper deposit using advanced integration of geological, remote sensing, geochemical, and magnetics data. Journal of Mining and Environment, 9: 19-39.

Barak, S., Imamalipour, A., Abedi, M., 2023. Application of Fuzzy Gamma Operator for

Mineral Prospectivity Mapping, Case Study: Sonajil Area. Journal of Mining and Environment, 14: 981-997.
Barak, S., Imamalipour, A., Abedi, M., 2024. Employing multiple prospectivity mapping and exploration targeting, a case study from the Sonajil porphyry copper deposit, north-western Iran. Bulletin of Geophysics and Oceanography, DOI 10.4430/bgo00462.
Barak, S., Imamalipour, A., Abedi, M., Bahroudi, A., Mamikhalifani, F., 2021. Comprehensive modeling of mineral potential mapping by integration of multiset geosciences data. Geochemistry, 81: 125824.
Barbalace, K., 2007. Periodic table of elements. Environmental Chemistry. com, 04-14.
Berberian, M., King, G.C.P., 1981. Towards a paleogeography and tectonic evolution of Iran: Reply. Canadian Journal of Earth Sciences, 18: 1764-1766.
Carranza, E.J.M., Hale, M., 1997. A catchment basin approach to the analysis of reconnaissance geochemical-geological data from Albay Province, Philippines. Journal of Geochemical Exploration, 60: 157-171.
Cheng, Q., Agterberg, F.P., Ballantyne, S.B., 1994. The separation of geochemical anomalies from background by fractal methods. Journal of Geochemical exploration, 51: 109-130.
Ebrahimi, H., Barak, S., 2019. The comparison among two approaches of perimeter-concentration fractal and Exploratory Data Analysis (EDA) in geochemical exploration for Au element in North-western of Iran, 11th symposium of Iranian Society of Economic Geology, Ahvaz, Iran.
Ghasemi, S., Imamalipur, A., Barak, S., 2024. Application of Fractal Modeling for Accurate Resources Estimation in the Qarah Tappeh Copper Deposit, NW Iran. Journal of Mining and Environment, 15: 1563-1577.
Gutiérrez, M., Gómez, V.M.R., Herrera, M.T.A., López, D.N., 2012. Exploratory analysis of sediment geochemistry to determine the source and dispersion of Ba, Fe, Mn, Pb and Cu and in Chihuahua, Northern Mexico. Journal of Geography and Geology, 4: 26.
Hassani Pak, A.A., Sharafaddin, M., 2002. Exploration Data Analaysis, University of Tehran Press.
Hassanpour, S., Afzal, P., 2013. Application of concentration–number (C–N) multifractal modeling for geochemical anomaly separation in Haftcheshmeh porphyry system, NW Iran. Arabian Journal of Geosciences, 6: 957-970.
Heidari, S.M., Afzal, P., Sadeghi, B., 2024. Molybdenum and gold distribution variances within Iranian copper porphyry deposits. Journal of Geochemical Exploration, 261: 107471.
Hezarkhani, A., Seljouqi, S., 2016. Fractal and Multifractal Modeling of Geochemical Data, Amirkabir University of Technology (Tehran Polytechnic).
Imamalipour, A., 2009. Mineralogy and Geochemistry Study of Manganese-Iron Deposits in Ophiolitic Sediments North of Chaldoran, Northwest Iran, Iranian Journal of Crystallography and Mineralogy, pp. 3-14.
Imamalipour, A., Barak, S., 2019. Detection of promising area for exploring rare elements using Exploratory Data Analysis (EDA) in Zanjan area, 11th symposium of Iranian Society of Economic Geology, Ahvaz, Iran.
Liu, Y., Cheng, Q., Zhou, K., 2019. New insights into element distribution patterns in geochemistry: A perspective from fractal density. Natural Resources Research, 28: 5-29.
Majidi, V., Ghalamghash, J., 2004. Geological Map Report of Siah Cheshmeh 1:100,000, Geological Survey and Mineral Explorations of Iran.
Mandelbrot, B.B., 1989. Fractal geometry: what is it, and what does it do?. Proceedings of the Royal Society of London. A. Mathematical and Physical Sciences, 423: 3-16.
Mandelbrot, B.B., 1982. The fractal geometry of nature, New York: WH freeman. 1: 25-74.
Momeni, M., Faal Qayoumi, A., 2012. Statistical Analyses Using SPSS, Ganj Shayegan Publications.

Nabavi, M.H., 1976. An introduction to the geology of Iran, Geological Survey and Mineral Exploration of Iran press.
Nogole-Sadat, M.A.A., Almasian, M., 1993. Tectonic map of Iran, scale 1: 1000, 000. Geological Survey of Iran, Tehran.
Paravarzar, S., Mokhtari, Z., Afzal, P., Aliyari, F., 2023. Application of an approximate geostatistical simulation algorithm to delineate the gold mineralized zones characterized by fractal methodology. Journal of African Earth Sciences, 200: 104865.
Pourgholam, M.M., Afzal, P., Adib, A., Rahbar, K., Gholinejad, M., 2024. Recognition of REEs anomalies using an image Fusion fractal-wavelet model in Tarom metallogenic zone, NW Iran. Geochemistry, 84: 126093.
Sadeghi, B., 2021. Concentration-concentration fractal modelling: a novel insight for correlation between variables in response to changes in the underlying controlling geological-geochemical processes. Ore Geology Reviews, 128: 103875.
Sanchez Siachoque, C.L., 2023. Geochemical Mapping of the North-Central Portion of the Yukon-Tanana Upland, Alaska, United States: Application of Exploratory Data Analysis (EDA) to REE and PGE Mining Prospection (Doctoral dissertation, Politecnico di Torino).
Shuguang, Z., Kefa, Z., Yao, C., Jinlin, W., Jianli, D., 2015. Exploratory data analysis and singularity mapping in geochemical anomaly identification in Karamay, Xinjiang, China. Journal of Geochemical Exploration, 154: 171-179.
Tukey, J.W., 1977. Exploratory data analysis, Reading, MA: Addison-wesley2: 131-160.
Xie, S., Bao, Z., 2004. Fractal and multifractal properties of geochemical fields. Mathematical Geology, 36: 847-864.
Yousefi, M., Barak, S., Salimi, A., Yousefi, S., 2023. Should geochemical indicators be integrated to produce enhanced signatures of mineral deposits? A discussion with regard to exploration scale. Journal of Mining and Environment, 14: 1011-1018.
Yousefi, M., Kamkar-Rouhani, A., Carranza, E.J.M., 2012. Geochemical mineralization probability index (GMPI): a new approach to generate enhanced stream sediment geochemical evidential map for increasing probability of success in mineral potential mapping. Journal of Geochemical Exploration, 115: 24-35.
Yousefi, M., Kamkar-Rouhani, A., Carranza, E.J.M., 2014. Application of staged factor analysis and logistic function to create a fuzzy stream sediment geochemical evidence layer for mineral prospectivity mapping. Geochemistry: Exploration, Environment, Analysis, 14: 45-58.
Yusta, I., Velasco, F., Herrero, J.M., 1998. Anomaly threshold estimation and data normalization using EDA statistics: application to lithogeochemical exploration in Lower Cretaceous Zn–Pb carbonate-hosted deposits, northern Spain. Applied geochemistry, 13: 421-439.
Zuo, R., Wang, J., 2016. Fractal/multifractal modeling of geochemical data: A review. Journal of Geochemical Exploration, 164: 33-41.